学位申請論文

Tunnel barrier formation in multi-wall carbon nanotubes

（多層カーボンナノチューブへの
トンネル障壁作製に関する研究）

平成 29 年 9 月

Hiroshi Tomizawa
富沢　啓

Acknowledgment

I would like to thank Prof. K. Ishibashi for giving me the opportunity to do research at RIKEN. I have learned so many things from discussions. I would like to thank Prof. H. Takayanagi who is my thesis chief examiner. I would like to thank Dr. T. Yamaguchi for discussions and helpful advices in sample fabrication and low temperature measurements. I would like to thank Prof. S. Akita for providing high quality multi-wall carbon nanotubes. I would like to thank Mr. M. Mihara for his technical support and machine maintenance. I would like to thank Ms. Y. Asano, Ms. Y. Sakai, and Ms. K. Nakanishi for their kind help. I would like to thank all my colleagues met in RIKEN and Tokyo University of Science.

Abstract

This thesis describes experimental results about tunnel barrier formation in multi-wall carbon nanotubes (MWNTs) and transport measurements through formed tunnel barriers. In the realization of integrated single electron transistor circuits or multiple quantum dot (QD)-based devices, carbon nanotubes are attractive bottom-up nanomaterial for building blocks owing to their small diameter. Single-wall carbon nanotubes (SWNTs) are an ideal material owing to its extreme small diameter and intensive studies have been carried out. Since tunnel barriers are formed at the metal/SWNT interface, SWNT QDs can be fabricated by only depositing metallic contacts. In many cases, however, unwanted barriers are also formed in the channel of the SWNT by resist processes or charge impurities on the substrate, and multi-dot behaviors are observed. The barriers, including contact interfaces, are basically uncontrollable and to greatly reduce the yield of device fabrication. MWNTs are, on the other hand, robust to resist processes compared with the SWNTs and Ohmic behavior is observed even at liquid He temperature.

In this thesis, we have developed two kinds of tunnel barrier formation technique in the MWNTs. One is resist opening and the other is focused ion beam. The MWNTs, grown by an arc discharge method, were dispersed on the chip and located by the atomic force microscopy. Two terminal resistance of the MWNTs contacted by Pd with a gap of 1 μm is 10 - 20 kΩ in most of samples. Current - voltage characteristic is linear even at 1.5 K.

In resist opening technique, electron beam resist is applied on the contacted

MWNT samples and a narrow opening of 50 nm is formed on the MWNT. Then, the entire substrate is irradiated by Ar beam. Coupled dot fabrication was successfully demonstrated with serial triple barriers. However, the resistance after irradiation varied greatly and the reproducibility was too low for device fabrication by the technique at present in conclusion.

In focused ion beam technique, Ga ion beam with a diameter of approximately 10 nm was irradiated to the MWNTs. The resistance changes were reasonably reproducible and showed ion dose dependence with some variation. We consider a part of the variation was owing to the diameter variation. Irradiated MWNTs on a grid were observed by transmission electron microscope and the region formed amorphous-like structures. Height of the tunnel barriers was estimated by the temperature dependence and the bias-voltage dependence of the current through single barriers. Single electron transport was demonstrated in double barrier samples and the single-dot behaviors were observed in four tenths of samples. The reproducibility was much improved and high enough for device fabrication.

In conclusion, we have developed the tunnel barrier formation technique. By using focused ion beam technique, we can fabricate the tunnel barriers with controlling positions, numbers and height. The single-dot samples can be fabricated with high reproducibility. Moreover, the technique can form tunnel barriers in suspended MWNTs because resist process is not required. The present technique can be applied to fabricate integrated single electron transistor circuits or electromechanical resonators using MWNTs.

Chapter 1

Introduction

1.1 Background

Tunneling is one of the quantum mechanical phenomenon which cannot be explained by classical mechanics. In 1957, L. Esaki, *et al*. demonstrated the tunneling devices in semiconductor *p*-*n* junction devices [1]. Thereafter, progress of fine processing technology and thin film lamination technology have made it possible to confine electrons to two-dimensional, one-dimensional, and zero-dimensional structures. In zero-dimensional structure, electrons are confined in small island and electrons move into and out of the island by tunneling. Single electron tunneling devices have been realized for the first time in metals [2]. In addition to very low power consumption, various kind of devices have been studied for example of single electron turnstile [3], pump [4,5], memory [6,7], and quantum

cellular automata [8]. Electrons in zero-dimensional structure have discrete energy owing to quantum confinement effect. Semiconductor zero-dimensional structures, called quantum dots (QDs), also extensively studied [9-20]. Single electron devices have been also realized in bottom-up approach of using self-assembled semiconductors [21-25] and carbon nanomaterials. Carbon nanotubes (CNTs), discovered by S. Iijima in 1991 [26], consist of graphite sheets wrapped into cylindrical tubes. Multi-wall carbon nanotubes (MWNTs) are comprised an array of nanotubes that are concentrically nested and single-wall carbon nanotubes (SWNTs) have only a single layer [27]. CNTs have a few micro meters' length. Therefore, source/drain contacts can be easily fabricated by conventional lithography technique and transport properties have been extensively studied [28-34].

As a building block for single electron transistors and QD-based devices, CNTs are attractive materials owing to their extreme small diameter. In the case of SWNT, Schottky tunnel barriers are formed at the interface between the SWNT and the metal by depositing metallic contacts on an individual SWNT for the source/drain electrodes, and the entire SWNT between the contacts is expected to work as a single QD at low temperatures [35-36]. Another method to define tunnel barriers is using electrostatic gates [37-40]. In SWNT QDs, however, unwanted barriers are easily produced in the channel of the SWNTs by damage or defects induced during fabrication and/or by charged particles that may reside near the SWNT on a substrate. As a result, multi-dot behaviors are observed in many cases

[41,42]. Although the ultraclean SWNTs have been realized by growing them on a suspended or trench structure [43-46], the methods are not flexible enough to fabricate integrated nanodevices or circuits with multiple QDs. In the case of MWNTs, on the other hand, a practical advantage is robustness to the resist processes. Besides, the resistance of MWNT-metal junctions is lower and the tube-metal couplings are much stronger [47,48]. Therefore, development of tunnel barrier formation techniques is required to realize QD-based devices and circuits using MWNTs.

Ion beam irradiation techniques have attracted attention for this purpose for nanoscale materials such as carbon nanomaterials [49-55]. However, ion beam irradiation usually produces unwanted damage or defects, which, in turn, could produce a tunnel barrier in CNTs. In fact, tunnel barrier formation and single electron transport have been reported about SWNTs [56] and MWNTs [57]. In SWNTs, room temperature operation has been demonstrated. In MWNTs, discrete quantum levels have been observed at 10 K [58]. In addition, single electron inverters that could be a building block of logic devices have been demonstrated in MWNTs of which tunnel barriers are formed by Ar ion beam irradiation [59]. In the realization of more complex devices, the evaluation of various tunnel barrier formation processes is indispensable.

1.2 Single electron transport

In this section, single electron transport in single dots [16] and coupled double dots [19,60-62] is briefly explained.

1.2.1 Single dots

Figure 1.1 shows the model circuit of a single dot system. The dot is connected to the gate voltage V_G through the gate capacitance C_G, and to the source and drain voltage V_{SD} through the tunnel barriers. When an electron moves into the dot by tunneling, the charge of the dot is changed with the charging energy of $E_C = e^2/C_{total}$, where e is the elementary charge and C_{total} is the self-capacitance of the dot. To define the number of electrons on the dot, suppression of two fluctuations is required. If E_C is larger than the thermal energy of k_BT, where k_B is the Boltzmann constant and T is temperature, the thermal fluctuation is suppressed. The other is quantum fluctuation. If the tunnel barrier is transparent, the electrons on the dot are not located long enough time compared to the time scale of the measurement. Typical time scale to charge or discharge the dot is $\Delta t = R_t C_{total}$, where R_t is the tunnel resistance. The uncertainty relation $\Delta E \Delta t = (e^2/C_{total}) R_t C_{total} > h$, where h is the Planck constant, ins that R_t should be much larger than the quantum resistance $h/e^2 \approx 25.8\,\mathrm{k\Omega}$ .Therefore, two conditions to observe the single electron transport is required that the electrons flow one by one through the dot.

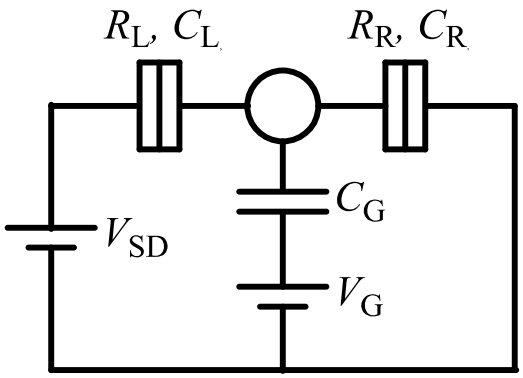

Fig. 1.1. Equivalent circuit of the single dot system. The dot is connected to the gate voltage V_G through the gate capacitance C_G, and to the source and drain voltage V_{SD} through the tunnel barriers.

$$\frac{e^2}{C_{\text{total}}} \gg k_B T$$

$$R_t \gg \frac{h}{e^2}$$

Figure 1.2 (a) shows the differential conductance plot as functions of V_G and V_{SD}. The serial gray rhombuses are called Coulomb diamonds and the inside of the diamonds corresponds to the Coulomb blockade state. The number of electrons on the dot is exactly different by one from adjacent diamonds. Figure 1.2 (b) shows the current with small V_{SD} as a function of V_G. The current flows at only the contact point between the diamonds. The regular current peaks called Coulomb oscillation.

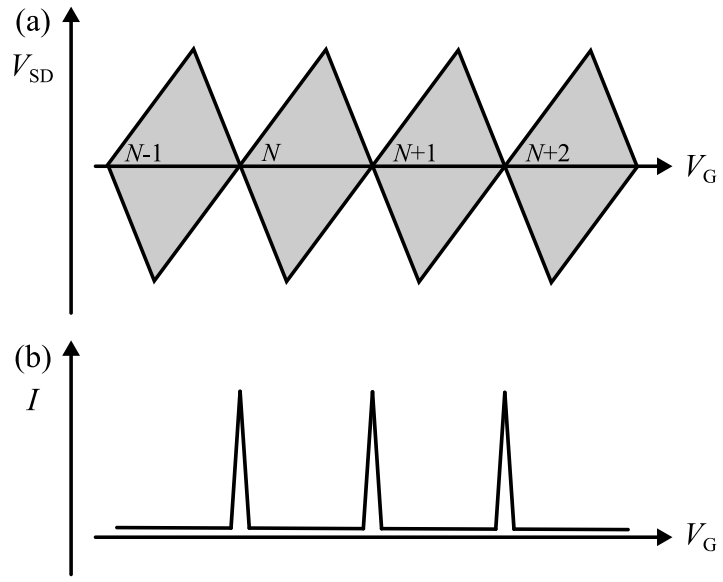

Fig. 1.2. (a) Differential conductance plot as functions of V_G and V_{SD}. The charge stability diagram is called Coulomb diamonds. N is the number of the electrons on the dot. (b) Current with small V_{SD} as a function of V_G. The periodic current peaks are called Coulomb oscillation.

1.2.2 Double dots

Figure 1.3 shows the model circuit of a double dot system. Each dot is capacitively connected to the gate voltage $V_{G1(G2)}$ through the gate capacitance $C_{D1G1(D2G2)}$ and the cross-capacitance $C_{D2G1(D1G2)}$. The two dots are coupled to each other and to the source and drain voltage V_{SD} through the tunnel barriers. Although each dot is connected only to the respective gate voltage ideally, cross-capacitance is also coupled to the other dot depending on the actual sample structure.

Figure 1.4 (a) shows the current plot as functions of V_{G1} and V_{G2} with small

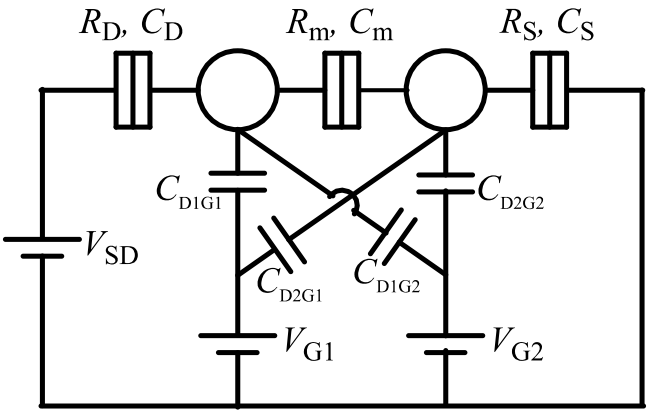

Fig 1.3. Equivalent circuit of the double dot system. Each dot is capacitively connected to gate voltage through capacitance and cross-capacitance. Two dots are coupled to each other by a tunnel junction.

V_{SD} called linear transport regime. The numbers of electrons are fixed within hexagonal region called honeycomb cells. The current flows at triple points that three charge states are in contact with each other. Figure 1.4 (b) shows the charge stability diagram with finite V_{SD} called nonlinear transport regime. The triple points spread to triangle sharp called bias triangle.

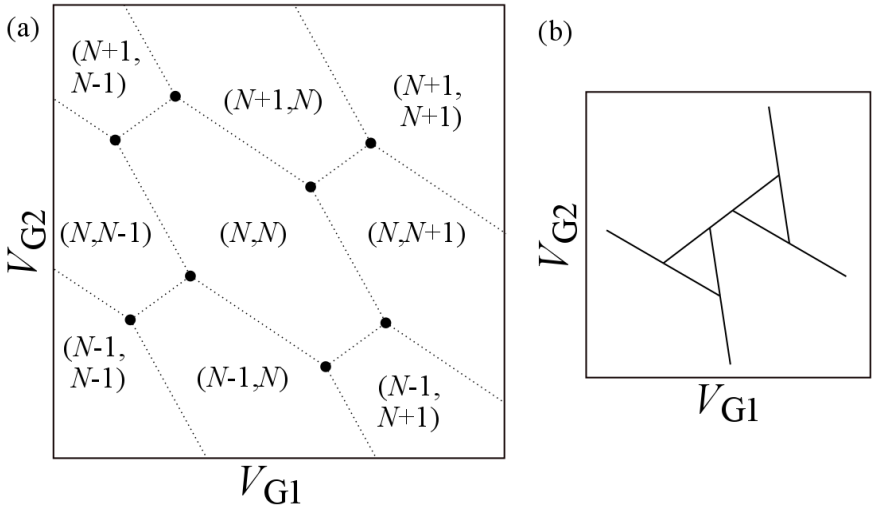

Figure 1.4. (a) Current plot as functions of two gate voltage in linear transport regime. The current flows at triple points that three honeycomb cells are in contact with each other. (b) The triple points spread to bias triangles in nonlinear transport regime.

1.3 Purpose

Purpose of this thesis is to develop tunnel barrier formation technique in MWNTs. In the realization of integrated single electron transistor circuit and multiple QD-based devices, high reproducibility and controllability of the tunnel barrier formation are important. Formed tunnel barriers will be characterized by transport measurement. Fabrication of double and triple barrier samples will be demonstrated by using the techniques, and single electron transport in the samples will be presented.

1.4 Outline

In chapter 1, background of this thesis and single electron transport in equivalent circuits of single and coupled double dot systems are presented. Then, purpose of this thesis is mentioned.

In chapter 2, device fabrication methods and basic transport characteristics of the multi-wall carbon nanotube devices are discussed. The multi-wall carbon nanotubes are grown by an arc discharge method and dispersed on a chip. The devices are fabricated by the conventional lift-off processes. Transport measurements are carried out in probe system at room temperature and in ^{4}He cryostat at low temperatures.

In chapter 3, tunnel barrier formation by using resist opening technique is demonstrated and the formed tunnel barriers are characterized. Coupled double dot transport in serial triple barrier samples is demonstrated.

In chapter 4, tunnel barrier formation by using focused ion beam technique is demonstrated. The dose dependence of the barrier resistance and the correlation between the resistance and the barrier height is discussed. Irradiated regions are characterized by transmission electron microscope. Single electron transport in double barrier samples is demonstrated and the yield of the sample fabrication is discussed.

In chapter 5, comparison of the two formation techniques, conclusion of this thesis, and future work are described.

Reference

[1] L. Esaki, Phys. Rev. **109**, 603 (1958).

[2] T. A. Fulton, and G. J. Dolan, Phys. Rev. Lett. **59**, 109 (1987).

[3] L. J. Geeligs, V. F. Anderegg, P. A. M. Holweg, J. E. Mooij, H. Pothier, D. Esteve, C. Urbina, and M. H. Devoret, Phys. Rev. Lett. **64**, 2691 (1990).

[4] H. Pothier, P. Lafarge, P. F. Orfila, C. Urbina, D. Esteve, and M. H. Devoret, Physica B, **169**, 573 (1991).

[5] H. Pothier, P. Lafarge, C. Urbina, D. Esteve and M. H. Devoret, Europhys. Lett. **17**, 249 (1992).

[6] K. Yano, T. Ishii, T. Hiramoto, T. Kobayashi, F. Mukai, and K. Seki, IEEE Tras. Electon Devices **41**, 1628 (1994).

[7] P. D. Dresselhaus, L. Ji, Siyuan Han, J. E. Lukens, and K. K. Likharev, Phys. Rev. Lett. **72**, 3226 (1994).

[8] I. amlani, A. O. Orlov, G. Toth, G. H. Bernstein, C. S. Lent, and G. L. Snider, Science, **284**, 289 (1999).

[9] M. Field, C. G. Smith, M. Pepper, D. A. Ritchie, J. E. F. Frost, G. A. C. Jones, and D. G. Hasko, Phys. Rev. Lett. **70**, 1311 (1993).

[10] S. Tarucha, D. G. Austing, T. Honda, R. J. van der Hage, and L. P. Kouwenhoven, Phys. Rev. Lett. **77**, 3613 (1996).

[11] M. Ciorga, A. S. Sachrajda, P. Hawrylak, C. Gould, P. Zawadzki, S. Jullian, Y. Feng, and Z. Wasilewski, Phys. Rev. B, **61**, R16315 (2000).

[12] L. P. Kouwenhoven, S. Jauhar, J. Orenstein, P. L. McEuen, Y. Nagamune, J.

Motohisa, and H. Sakaki, Phys. Rev. Lett. **73**, 3443 (1994).

[13] N. C. van der Vaart, S. F. Godijn, Y. V. Nazarov, C. J. P. M. Harmans, J. E. Mooij, L. W. Molenkamp, and C. T. Foxon, Phys. Rev. Lett. **74**, 4702 (1995).

[14] T. Fujisawa, T. H. Oosterkamp, W. G. van der Wiel, B. W. Broer, R. Aguado, S. Tarucha, and L. P. Kouwenhoven, Science **282**, 932, (1998).

[15] T. H. Oosterkamp, T. Fujisawa, W. G. van der Wiel, K. Ishibashi, R. V. Hijman, S. Tarucha, and L. P. Kouwenhoven, Nature (London) **395**, 873, (1998).

[16] L. P. Kouwenhoven, C. M. Marcus, P. L. Mceuen, S. Tarucha, R. M. Westervelt, and N. S. Wingreen, *Mesoscopic Electron Transport*, pp.105-214, Springer (1997).

[17] L. P. Kouwenhoven, D. G. Austing, and S. Tarucha, Rep. Prog. Phys. **64**, 701 (2001).

[18] W. G. van der Wiel, T. H. Oosterkamp, S. de Franceschi, C. J. P. M. Harmans, L. P. Kouwenhoven, *Strongly Correlated Fermions and Bosons in Low-Dimensional Disordered Systems*, pp.43-68, Springer (2002).

[19] W. G. vam der Wiel, S. De Franceschi, J. M. Elzerman, T. Fujisawa, S. Tarucha, and L. P. Kouwenhoven, Rev. Mod. Phys. **75**, 1 (2002).

[20] R. Hanson, L. P. Kouwenhoven, J. R. Petta, S. Tarucha, and L. M. K. Vandersypen, Rev. Mod. Phys. **79**, 1217 (2007).

[21] M. T. Björk, C. Thelander, A. E. Hansen, L. E. Jensen, M. W. Larsson, L. R. Wallenberg, and L. Samuelson, Nano Lett. **4**, 1621 (2004).

[22] C. Fasth, A. Fuhrer, M. T. Björk, and L. Samuelson, Nano Lett. **5**, 1487 (2005).

[23] Y. Hu, H. O. H. Churchill, D. J. Reilly, J. Xiang, C. M. Lieber, and C. M. Marcus, Nature Nanotechnol. **2**, 622 (2007).

[24] M. Jung, K. Hirakawa, Y. Kawaguchi, S. Komiyama, S. Ishida, and Y. Arakawa, Appl. Phys. Lett. **86**, 033106 (2005).

[25] K. Shibata, A. Umeno, K. M. Cha, and K. Hirakawa, Phys. Rev. Lett. **109**, 077401 (2012).

[26] S. Iijima, Nature, **352**, 56 (1991).

[27] S. Iijima, and T. Ichihashi, Nature, **363**, 603 (1993).

[28] M. Bockrath, D. H. Cobden, P. L. McEuen, N. G. Chopra, A. Zettl, A. Thess, and R. E. Smalley, Science 275, 1922 (1997).

[29] S. J. Tans, M. H. Devoret, H. Dai, A. Thess, R. E. Smalley, L. J. Geerligs, and C. Dekker, Nature, **386**, 474 (1997).

[30] M. Bockrath, D. H. Cobden, J. Lu, A. G. Rinzler, R. E. Smalley, L. Balents and P. L. McEuen, Nature **397**, 598 (1999).

[31] Z. Yao, H. W. Ch. Postma, L. Balents, and C. Dekker, Nature **402**, 273 (1999).

[32] J. Nygård, D. H. Cobden and P. E. Lindelof, Nature **408**, 342 (2000).

[33] W. Liang, M. Bockrath, D. Bozovic, J. H. Hafner, M. Tinkham, and H. Park, Nature **411**, 665 (2001).

[34] P. Jarillo-Herrero, J. A. van Dam and L. P. Kouwenhoven, Nature 439, 953 (2006).

[35] D. H. Cobden and J. Nygård, Phys. Rev. Lett. **89**, 046803 (2002).

[36] S. Moriyama, T. Fuse, M. Suzuki, Y. Aoyagi, and K. Ishibashi, Phys. Rev. Lett.

94, 186806 (2005).

[37] N. Mason, M. J. Biercuk, C. M. Marcus, Science, **303**, 655 (2004).

[38] H. I. Jørgensena, K. Grove-Rasmussen, J. R. Hauptmann, and P. E. Lindelof, Appl. Phys. Lett. **89**, 232113 (2006).

[39] M. R. Gräber, W. A. Coish, C. Hoffmann, M. Weiss, J. Furer, S. Oberholzer, D. Loss, and C. Schönenberger, Phys. Rev. B **74**, 075427 (2006).

[40] S. Sapmaz, C. Meyer, P. Beliczynski, P. Jarillo-Herrero, and L. P. Kouwenhoven, Nano Lett. **6**, 1350 (2006).

[41] M. Suzuki, K. Ishibashi, T. Ida, and Y. Aoyagi, Jpn. J. Appl. Phys. **40**, 1915 (2001).

[42] X. Zhou, J. Hedberg, Y. Miyahara, P. Grutter, and K. Ishibashi, Nanotechnology, **25**, 495703 (2014).

[43] P. Jarillo-Herrero, S. Sapmaz, C. Dekker, L. P. Kouwenhoven, and H. S. J. van der Zant, Nature, **429**, 389 (2004).

[44] J. Cao, Q. Wang, and H. Dai, Nature Materials **4**, 745 (2005).

[45] G. A. Steele, G. Gotz, and L. P. Kouwenhoven, Nature Nanotechnol. **4**, 363 (2009).

[46] J. Waissman, M. Honig, S. Pecker, A. Benyamini, A. Hamo, and S. Ilani, Nature Nanotechnol. **8**, 569 (2013).

[47] M. R. Buitelaar, A. Bachtold, T. Nussbaumer, M. Iqbal, and C. Schönenberger, Phys. Rev. Lett. **88**, 156801 (2002).

[48] A. Kanda, K. Tsukagoshi, Y. Aoyagi, and Y. Ootuka, Phys. Rev. Lett. **92**,

036801 (2004).

[49] A. V. Krasheninnikov, and F. Banhart, Nature Materials **6**, 723 (2007).

[50] M. Terrones, F. Banhart, N. Grobert, J.-C. Charlier, H. Terrones, and P. M. Ajayan, Phys. Rev. Lett. **89**, 075505 (2002).

[51] A. V. Krasheninnikov, K. Nordlund, and J. Keinonen, Appl. Phys. Lett. **81**, 1101 (2002).

[52] B. Q. Wei, J. D'Arcy-Gall, P. M. Ajayan, and G. Ramanath. Appl. Phys. Lett. **83**, 3581 (2003).

[53] M. S. Raghuveer, P. G. Ganesan, J. D'Arcy-Gall, G. Ramanath, M. Marshall, and I. Petrov, Appl. Phys. Lett. **84**, 4484 (2004).

[54] J. A. V. Pomoell, A. V. Krasheninnikov, K. Nordlund, and J. Keinonen, J. Appl. Phys. **96**, 2864 (2004).

[55] S. K. Pregler, and S. B. Sinnott, Phys. Rev. B **73**, 224106 (2006).

[56] K. Maehashi, H. Ozaki, Y. Ohno, K. Inoue, K. Matsumoto, S. Seki, and S. Tagawa, Appl. Phys. Lett. **90**, 023103 (2007).

[57] M. Suzuki, K. Ishibashi, T. Toratani, D. Tsuya, and Y. Aoyagi, Appl. Phys. Lett. **81**, 2273 (2002).

[58] D. Tsuya, M. Suzuki, S. Moriyama, Y. Aoyagi, and K. Ishibashi, Physica E, 24, 50 (2004).

[59] K. Ishibashi, D. Tsuya, M. Suzuki, and Y. Aoyagi, Appl. Phys. Lett. **82**, 3307 (2003).

[60] V. Hung Nguyen, V. Lien Nguyen, and H. Nam Nguyen, J. Appl. Phys. **96**,

3302 (2004).

[61] B.-K. Kim, M. Seo, S. U. Cho, Y. Chung, N. Kim, M.-H. Bae, and J.-J. Kim, Nanotechnology **25**, 295201 (2014).

[62] D. Taubert, D. Schuh, W. Wegscheider, and S. Ludwig, Rev. Sci. Instrum. **82**, 123905 (2011).

Chapter 2

Fabrication methods and basic transport characteristics of multi-wall carbon nanotube devices

This chapter will describe the fabrication methods of the multi-wall carbon nanotube devices and its basic characteristics of the transport. The device fabrication methods used in this thesis are conventional lift-off processes. Then, the basic transport characteristics of the multi-wall carbon nanotubes will be presented.

2.1 Substrate preparation

A highly-doped Si wafer with a thermally oxidized surface of 200 nm thickness was cut out into 20 mm square pieces by the diamond tip pen. The substrates were ultrasonically cleaned sequentially in acetone, 2-propanol, and deionized water for 5 min each and dried by N_2 blow. The substrate surface was then treated by the UV-ozone asher at 200℃ for 20 min to remove organic residues.

After the substrate cleaning, alignment marks were first defined. The high-resolution positive electron beam (EB) resist ZEP520A was applied onto the substrate with a rotational speed of 4000 rpm and then prebaked on the hotplate at 180 ℃ for 2 min. The alignment marks were drawn by the EB lithography system with an acceleration voltage of 100 kV and a dose of 150 μC/cm^2. The exposed pattern was developed in o-xylene for 6 min. Then 10 nm thickness of Ti and 300 nm thickness of Au were deposited via the EB evaporator and lifted-off in *N*-methyl-2-pyrrolidone (NMP) at 60 ℃ for 2 hours. In this process, 32 marks for each 16 chips, 2 marks for global alignment, and 1 mark as a landmark were fabricated. From this point forward, all processes were aligned by using these marks.

Address marks for location of MWNTs were then patterned. The EB resist was spin-coated again with a rotational speed of 6000 rpm and the address marks were written by the EB lithography system. Then 10 nm thickness of Ti was deposited via the evaporator and lifted-off in NMP. Figure 2.1 (b) shows a part of the address marks.

Bonding pads are required to connect the mesoscopic nanotube devices with the macroscopic measurement systems. The lift-off layer LOR3A was applied on the substrate with a rotational speed of 5000 rpm and prebaked on the hotplate at 180 ℃ for 5 min. Then the positive photolithography resist AZ1500 was spin-coated with a rotational speed of 5000 rpm and prebaked in the oven at 100 ℃ for 10 min. The bonding pads were exposed by the maskless lithography tool and developed by AZ 300 MIF developer for 80 sec. It should be noted that the AZ

developer is alkaline and able to destroy the thin Ti or Pd patterns. The developed processing substrates were post-baked in the oven at 100 ℃ for 10 min. Then 10 nm thickness of Ti and 80 nm thickness of Au were deposited via the EB evaporator and lifted-off in NMP. The size of the pad is 150 μm × 200 μm. In this process, cutoff pattern for dicing were fabricated at the same time. Figure 2.1 (a) shows the chip design.

The prepared substrates were covered by some resist to protect surface from the Si shavings, and then diced into 16 chips with the size of 3.84 mm × 3.6 mm by the scriber. The chips were cleaned by the UV-ozone asher to remove the resist residue and to activate the surface for nanotube dispersion.

2.2 Device fabrication

Multi-wall carbon nanotubes (MWNTs) used in this thesis were provided by Prof. Akita's group at Osaka Prefecture University, and grown by an electrical arc discharge method [1,2]. The diameter, the number of walls, and the length of the MWNTs are in the range of 10-20 nm, 8-20 walls, and around 5 μm respectively, estimated by transmission electron microscopy (TEM). Figure 2.2 shows the typical TEM image of the MWNT. The as-prepared MWNTs were dispersed into 2-propanol and sonicated for hours. The prepared chip was dipped into the MWNT dispersion and then dried by N_2 blow. The atomic force microscope (AFM) was used to record the position of each MWNT relative to the predefined address marks (Fig 2.1 (b)) on the substrate. The number of individual MWNTs in a 600-μm^2 area

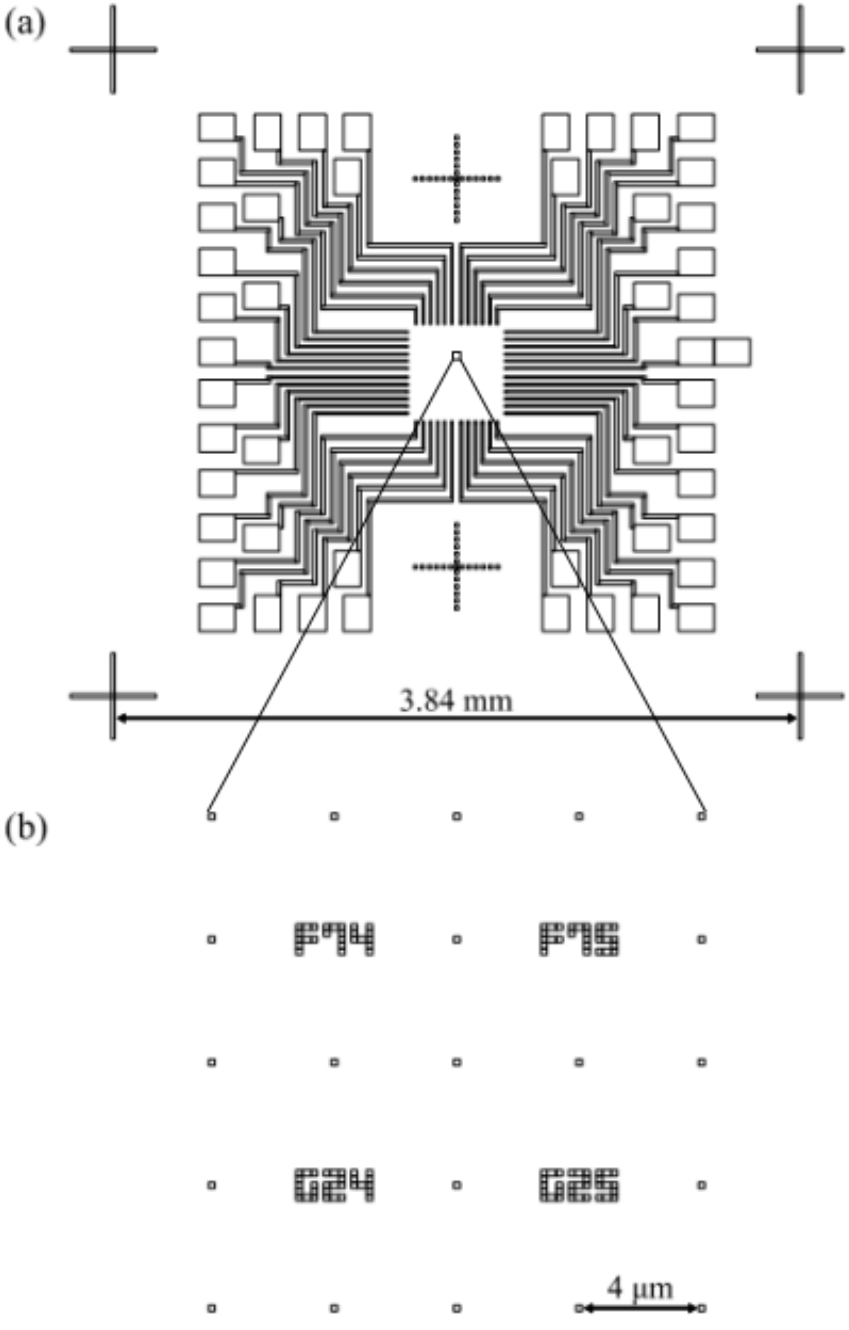

Figure 2.1. CAD design (a) 48-bonding line chip. (b) A part of the address marks.

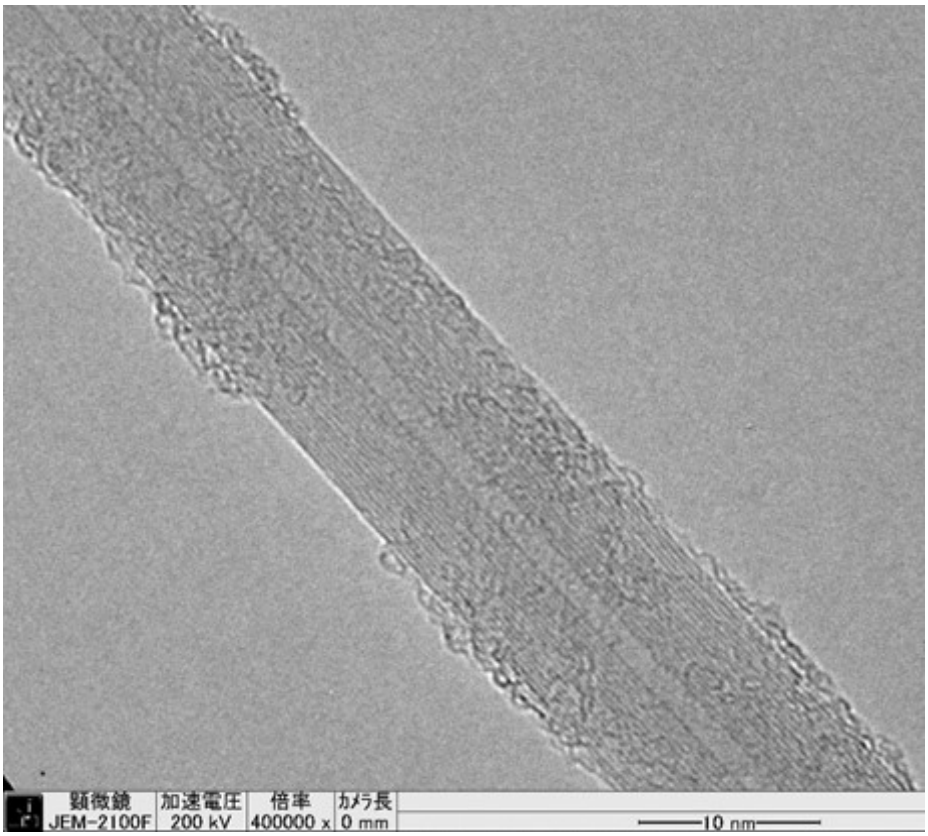

Figure 2.2. Typical transmission electron microscope image of the multi-wall carbon nanotube used in this study. The acceleration voltage was 200 kV and the magnification was 400,000.

observed on the substrate was in the order of ten in the present experimental condition. Source/drain contacts were designed by using the computer-aided design software AutoCAD. The designed contacts were patterned by EB lithography, depositing 30 nm of Pd, and the lift-off process. Figure 2.3(a) shows a SEM image of the fabricated device.

2.3 Measurement setup

2.3.1 Wire bonding

The fabricated sample was mounted on a ceramic chip carrier using Ag paste that connects conducting backside of the chip to the carrier for applying back-gate voltage. The bonding pads on the chip and the package pins were connected with Al wires by using the ultrasonic wedge-bonding tool. Figure 2.3(b) shows a picture of a mounted sample.

2.3.2 Transport measurement setup

Room temperature measurements were carried out at the probe measurement system under atmospheric conditions. The sample before bonding was fixed on the stage by vacuum. The bonding pads were touched by the probes and the source/drain voltage was applied to the sample through there. The resistance change between before and after beam irradiation was noted and appropriate samples were selected for low temperature measurement.

Low temperature measurements were carried out in the liquid ^{4}He refrigerator.

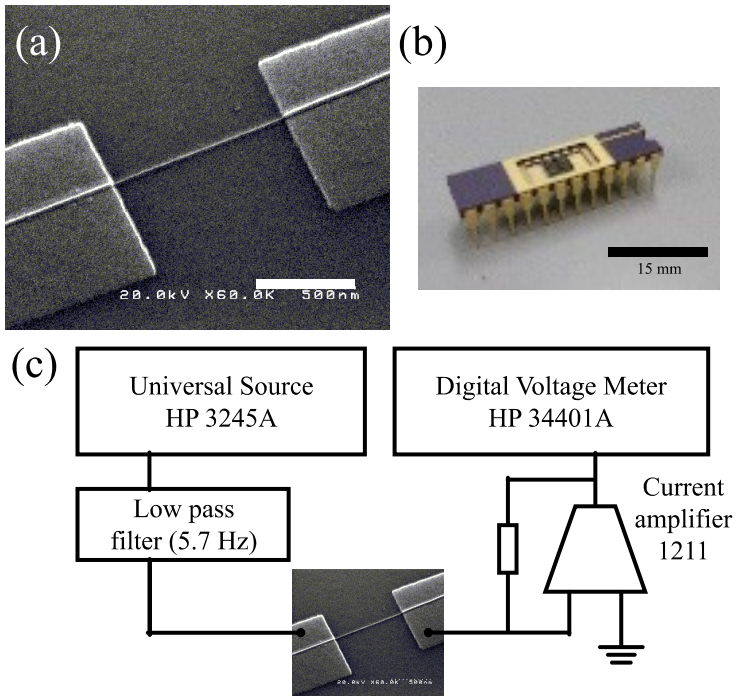

Figure 2.3. (a) Scanning electron microscope of the fabricated sample. The gap distance is 1 μm. The scale bar indicates 500 nm. (b) Picture of the mounted sample. The scale bar indicates 15 mm. (c) Schematics of the measurement system.

Liquid He flows into the sample chamber through needle valve and the sample chamber cools down to 1.5 K. An external voltage source HP3245A is connected to a contact by a 10-kΩ low pass filter with a cut-off frequency of 5.8 Hz. The current flows to the sample, the other contact, a current amplifier 1211, a digital voltage meter HP 34401A, and to ground. Figure 2.3 (c) shows a schematic diagram of the measurement system.

2.4 Transport characteristics

2.4.1 Transport characteristics at room temperature

The room temperature resistance of the fabricated samples was measured using a DC two-terminal method at the probe measurement system. Figure 2.4 shows a histogram of the resistance for 300 samples contacted by Pd [3,4]. The distance between source/drain contacts was 1 μm for all samples. The resistance values were concentrated within a small range, mainly 10-20 kΩ.

The resistance of the contacted MWNTs is reproducible while the MWNTs were not purified, mixed of metallic and semiconducting layers, and the layer number of each MWNTs was not the same. The reproducibility is one of the advantage over the single-wall carbon nanotubes.

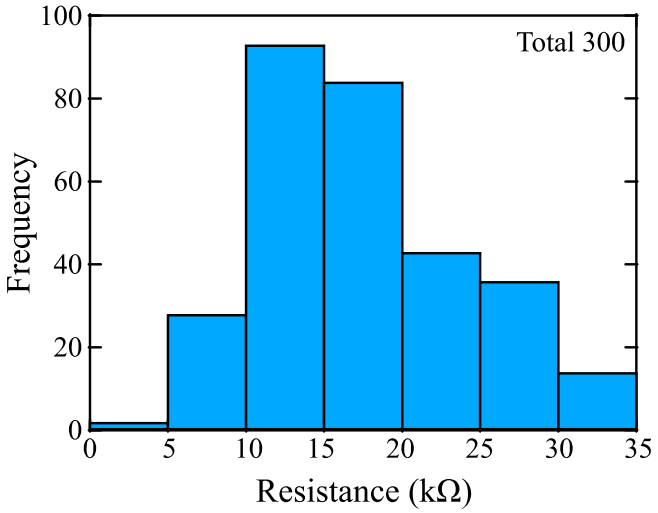

Figure 2.4. Histogram of the resistance of the multi-wall carbon nanotube samples. The sample number was 300 in total. The source/drain contacts were Pd with a gap distance of 1 μm.

2.4.2 Transport characteristics at low temperature

The mounted sample was loaded in the fridge and measured at the low temperature of 1.5 K. Figure 2.5 shows the I-V_{SD} curves at room temperature and 1.5 K. The I-V_{SD} curves showed still linear behavior even at 1.5 K. Furthermore, the change in resistance during cool down was only a few kΩ. The linear characteristic at 1.5 K suggests that the contact resistance at the metal-MWNT interface and the disorders in the MWNTs were transparent and Ohmic even at low temperature. The linearity has an advantage as a building block of nanodevices.

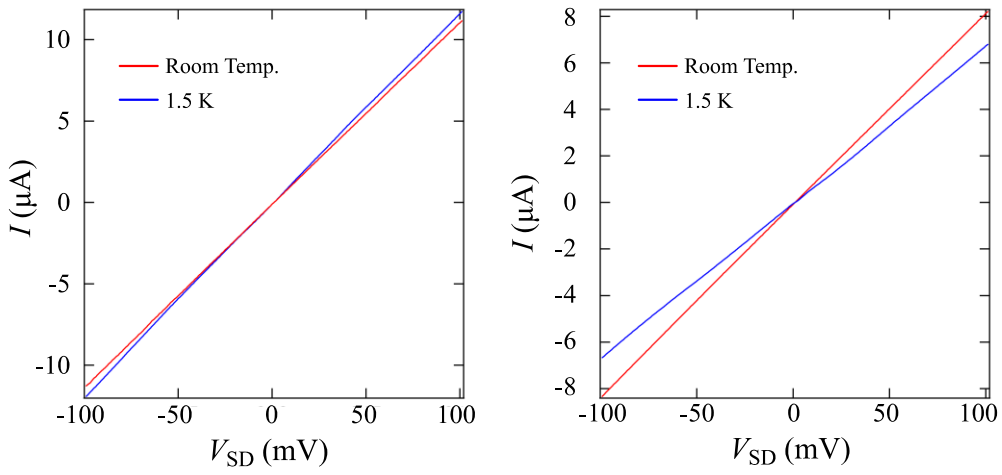

Figure 2.5. Typical current versus source-drain voltage characteristics of the non-irradiated multi-wall carbon nanotube devices. The red curve was measured at room temperature and the blue one at 1.5 K.

Reference

[1] S. Iijima, Nature **354**, 56 (1991).

[2] T. W. Ebbesen, and P. M. Ajayan, Nature **358**, 220 (1992).

[3] A. Javey, J. Guo, Q. Wang, M. Lundstrom, and H. Dai, Nature **424**, 654 (2003).

[4] Z. Chen, J. Appenzeller, J. Knoch, Y. Lin, and P. Avouris, Nano Lett. 5, 1497 (2005).

Chapter 3

Tunnel barrier formation by using resist opening technique

This chapter will describe tunnel barriers induced in individual multi-wall carbon nanotubes (MWNTs) by an Ar atom beam irradiation through resist opening. In this technique, as a result, the resistance values after irradiation have poor reproducibility. The height of the formed barriers was estimated from Arrhenius plot and Fowler-Nordheim plot. The fabrication technique was used to produce coupled double quantum dots with serially formed triple barrier on a MWNT.

3.1 Introduction

In this chapter, tunnel barriers were formed in individual MWNTs using an Ar atom beam irradiation process as one of the possible methods, and the characteristics of the fabricated barrier were evaluated by measuring the two-

terminal resistance of an individual MWNT with a single irradiated region. The obtained temperature and bias voltage dependence of the current curves made it possible to understand the transport mechanism through the formed barrier. We applied this technique to fabricate double quantum dots (DQDs) with triple barrier. The charge stability diagram at low temperature showed a honeycomb pattern that suggested the formation of a DQD [1]

3.2 Experimental

The MWNT sample was prepared as explained in chapter 2. A resistive Si substrate (>10,000 Ωcm) was used instead of a Si/SiO_2 substrate in this chapter. First, the sample was coated by the EB resist ZEP520A-7. The resist is diluted ZEP520A to 7 times and the thickness is 180 nm with a speed of 8000 rpm. To form a tunnel barrier, a narrow opening with a width of 50 nm was fabricated in the resist layer using electron beam lithography with an acceleration voltage of 100 kV. In this condition, the openings were designed to 30 nm width but the actual width after development was 50 nm. The MWNT was irradiated with an Ar atom beam accelerated with 2 kV for 90 s through the opening. The irradiation dose used to form the tunnel barriers shown in the later section was 2×10^{14} atoms/cm^2 and the number of atoms hit the MWNT was estimated at about 10^3 atoms.

In the present experiment, an Ar atom beam was used rather than the Ar ion beam used in our previous experiment [2]. In fact, when the Ar ion beam irradiation technique was applied to the fabrication of the present MWNTs with similar

conditions to those used in the previous experiment (300 V, 6×10^{16} ions/cm^2), we found that the irradiated regions were so easily sputtered that it was difficult to form an appropriate tunnel barrier. We do not know the clear reason for this difference, but we noticed that the effect of the irradiation depended on the details of the MWNTs, such as how they were grown, for example, by CVD or arc discharge, which may produce MWNTs of different qualities. Besides, even MWNTs grown by the same method may have different microscopic details. Further systematic study is necessary to understand the effect of ion beam irradiation effects.

Two types of samples were prepared: samples with a single tunnel barrier and samples with triple tunnel barrier. Figure 3.1 shows a scanning electron microscope image of the latter sample. The two metal electrodes (source and drain) are attached to the ends of the MWNT. The three red rectangular areas between the source/drain contacts indicate the Ar beam irradiated region where the tunnel barriers were expected to be formed. The inset of Fig. 3.1 displays a schematic cross-sectional view of the sample structure under irradiation. The two regions of the MWNT enclosed by the red lines were expected to work as coupled DQDs. The two gate electrodes were fabricated to control the electrochemical potential of each dot. To confirm the formation of the coupled DQDs and to characterize them, the current was measured using each gate with small and large source/drain voltages that called charge stability diagram measurements.

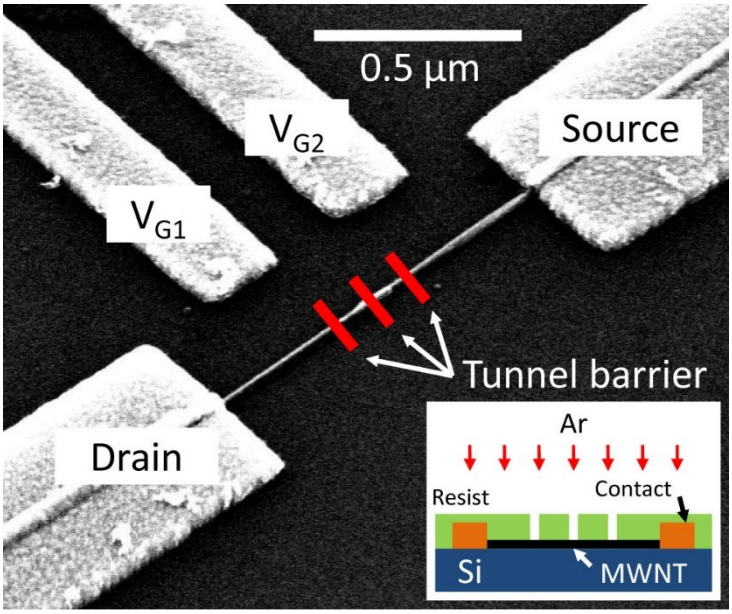

Figure 3.1. Scanning microscope image of the fabricated triple barrier sample. The source/drain electrodes and two gate electrodes were formed simultaneously by depositing Pd/Au. Three red regions schematically indicate the irradiated areas. Inset: schematic cross-sectional view of the sample structure under Ar irradiation. The resist layer with a thickness of 180 nm had three 50-nm wide openings on the multi-wall carbon nanotube.

3.3 Characterization of single barriers

3.3.1 Resistance change

Figure 3.2 shows a histogram of the room temperature linear resistance after Ar beam irradiation for single barrier samples fabricated on the same chip. The distance between source/drain contacts was 1 μm for all samples. While the resistance values were concentrated within a small range before the irradiation (Fig. 3.4), the values measured after the irradiation varied greatly from sample to sample even though they were irradiated at the same time. In most samples, the resistance increased or became too high to obtain a measurable current. Although we examined different conditions (beam acceleration voltage and irradiation time), a similar tendency was observed. As a result, it has to be admitted that the present process does not have sufficient reproducibility and complete reliability. It could be reasonable if unknown damages were produced in the irradiated region, which was not controlled in this work. Even so, a few samples had a resistance appropriate for the formation of quantum dots, a few hundreds of kΩ, which is larger than the quantum resistance. It is to be noted that the current that flowed through the resistive Si substrate could be ignored.

3.3.2 I-V_{SD} characteristics at various temperatures

Figures 3.3(a)-3.3(c) shows the resistance measurement results for three single-barrier samples with different room-temperature resistances. The resistance at room temperature was 52 kΩ (sample A), 112 kΩ (sample B), and 581 kΩ

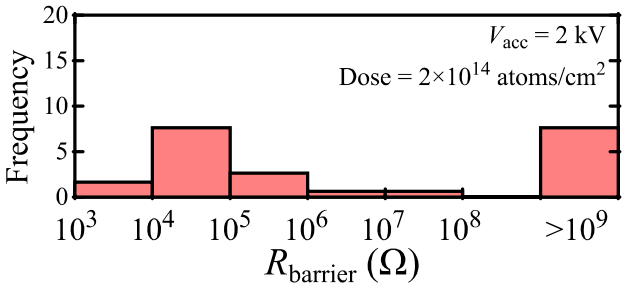

Figure 3.2. Histogram of resistance at room temperature after Ar beam irradiation for the 23 samples. The resistance values became widely distributed after the irradiation.

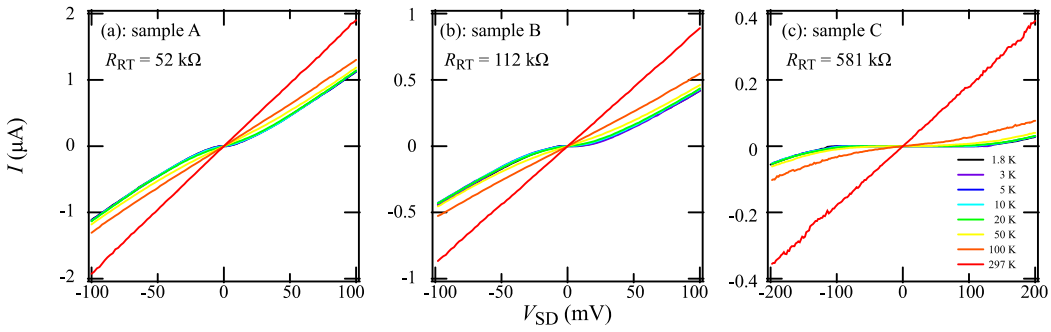

Figure 3.3. Current-voltage curves measured from 1.8 K to a room temperature of 297 K for three different samples having room temperature resistance R_{RT} of 52 kΩ (sample A), 112 kΩ (sample B), and 581 kΩ (sample C). The curves show non-linear behavior at 1.8K and linear behavior at high temperatures.

(sample C). The temperature dependence of the current-source-drain voltage (I-V_{SD}) curves is depicted in Figs. 3.3(a)-3.3(c) for samples A, B, and C, respectively, from 1.8K to room temperature (297 K). It is clear from Figs. 3.3(a)-3.3(c) that the I-V_{SD} curves of all of the samples became non-linear as the temperature was decreased but were linear at room temperature.

3.3.3 Temperature dependence

Figures 3.4(a)-3.4(c) show currents at fixed V_{SD} of 2 mV plotted in a logarithmic scale as a function of inverse temperature for samples A, B, and C, respectively (Arrhenius plot). It is obvious that there were two temperature regions in all plots [3]. At low temperatures, the current was almost independent of temperature, while at high temperatures the temperature dependence followed Arrhenius' law.

This behavior is well described by the following. At low temperatures, the current through the barrier at the damaged region was dominated by the tunneling process independent of the temperature, as indicated by the right inset of Fig. 3.4(c). As the temperature was increased, the current caused by carriers that overcame the barrier became dominant as indicated by the left inset of Fig. 3.4(c).

In the cases of samples A and B, the thermally excited current appeared to be dominant above 3 K. It is therefore suggested that the barriers were not high enough and the thermally excited current was still dominant even at a few Kelvin. For sample C, in contrast, the tunneling and thermally excited regions were well

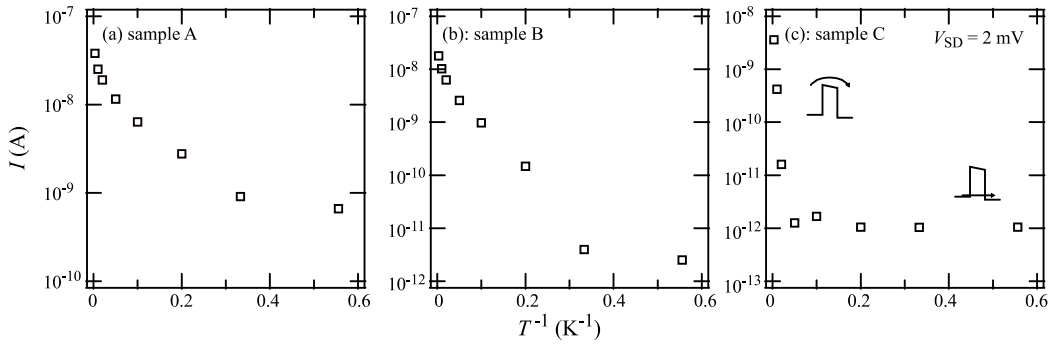

Figure 3.4. Plots of current versus inverse temperature for sample A, B, and C at small bias voltage of 2 mV. In the cases of sample A and B, the thermally excited carriers dominate the current through the barrier above 3 K because the barriers are not high enough compared to the thermal energy. In the sample C, the tunneling is dominant up to around 20K because the tunnel barrier is high enough compared to the thermal energy at 20K (1.7 meV).

distinguished. The tunneling current was dominant up to 20 K. These results do not contradict the above-mentioned picture, suggesting a higher tunneling barrier for sample C. The height of the tunnel barriers Φ estimated from the slope above 50 K in the thermally excited regime in the Arrhenius plot is Φ ~ 3.5, 5.3, and 2.8 × 10 meV for samples A, B, and C, respectively.

For samples A and B, it is to be noted that the Arrhenius plot seemed to have two different slopes. This was probably caused by the shapes of the barriers produced by Ar atom irradiation, which would not have been simple rectangles, but more complicated reflecting the microscopic structure of the induced damage. The presence of several potential islands in the barriers along the current flow might

cause the Arrhenius plot to have multiple slopes, in particular, when the barrier height is comparable to the bias voltage.

3.3.4 Bias voltage dependence

Figures 3.5(a)-3.5(c) show natural logarithm of current over square voltage against inverse voltage at lowest temperature of 1.8 K for sample A, B, and C, respectively (Fowler-Nordheim plot) [4]. In Figs 3.5(b) and 3.5(c), there are two voltage regions separated at a transition voltage V_{trans} indicated by arrows.

On the assumption that the barrier shape is rectangular at zero bias voltage, the barrier forms a trapezoidal shape in low bias region less than V_{trans}. In this region, the thickness of the barrier does not depend on the voltage and the electrons can flow only by a direct tunneling, as indicated by the right inset of Fig. 3.5(c). When the bias voltage becomes larger than the tunnel barrier height, the effective thickness of the tunnel barrier decreases by the degree of slope of the barrier and the electrons tunnel through triangle potential called Fowler-Nordheim (FN) tunneling, as indicated by the left inset of Fig. 3.5(c). Therefore, the changing point that divides the two kind of tunneling reflects the height of the tunnel barrier [5-8].

In the case of sample B and C, the transition voltage is $V_{\mathrm{trans}} \sim 5$ and ~ 51 mV, respectively. For sample A, there no changing point appeared. we considered that the V_{trans} was less than the minimum bias voltage of 2 mV of this measurement.

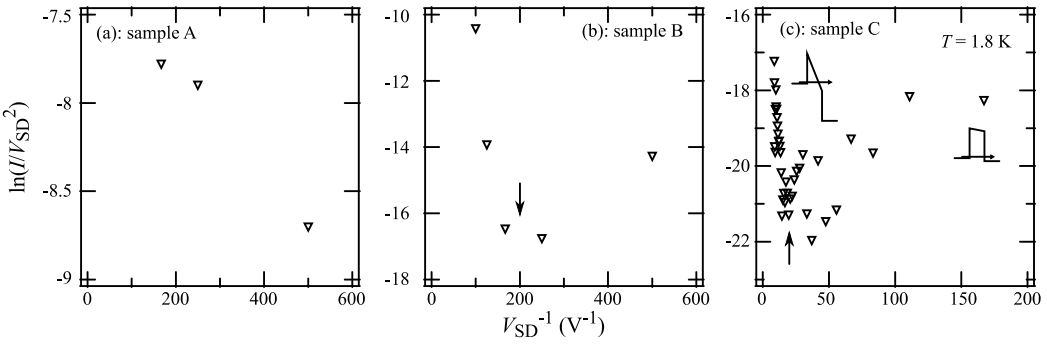

Figure 3.5. Plot of natural logarithm of current over square voltage against inverse voltage for sample A, B, and C at low temperature of 1.8 K. In the cases of sample B and C, the tunneling mechanism was changed at the voltage point indicated by the arrow. For sample A, the tunnel barrier height was expected to less than 2 mV.

3.3.5 Barrier height estimation

Figure 3.6 shows the estimated barrier height Φ and eV_{trans} as a function of the room temperature resistance. The values seem to have a positive correlation with the resistance at room temperature. For sample B, in addition, the values estimated from two method have a good agreement. For sample C, in contrast, the values are much different.

To use the present Ar atom beam irradiation method to form a tunnel barrier in the quantum dots, the height of the barrier should be greater than the other energy scales such as the thermal energy (k_{B}T), the quantum level spacing, and the charging energy. Based on our estimate of the charging energy of the dots in a later section (several meV), the barrier height of samples A and B would not be sufficient for the operation of the double dots, while that of sample C would be. In our arguments,

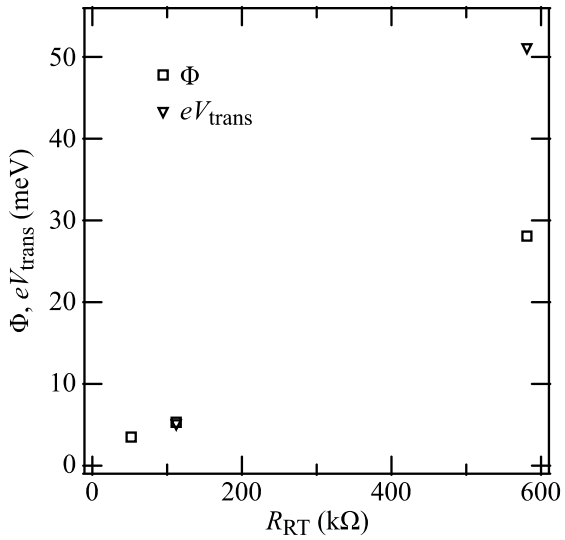

Figure 3.6. the estimated barrier height Φ and eV_{trans} as a function of the room temperature resistance. The barrier height seems to have a positive correlation with the resistance. For sample B, in addition, the values estimated from two method have a good agreement. For sample C, in contrast, the values are much different.

we simply assume that the tunnel barrier formed by the irradiation had a fixed width and a varying height. The width could be determined by the size of opening of the resist mask if serious damage did not penetrate in the lateral direction along the nanotube. In that case, the resistance variations very likely arose from the variation in the barrier height caused by the fluctuation of the produced damage in the irradiated area. At this moment, we do not know the microscopic nature of the produced damage. At the present stage, the variation is too large to use the method as a reliable and reproducible device process. To reduce the variation to a practically allowable level, it is necessary to understand the microscopic nature of the produced

damage and how it behaves upon further treatment such as thermal annealing.

3.4 Coupled double quantum dots

We fabricated coupled DQDs in MWNTs using the present technique. The sample structure is shown in Fig. 3.1: the MWNT had three barriers in series separated by a distance of 130 nm, and two side gates were also fabricated on the substrate surface. The room temperature resistance increased from 14 kΩ to 161 kΩ after the Ar atom irradiation. Figure 3.7(a) presents the experimental charge stability diagram of the triple barrier sample. The current as a function of the side gate voltages, V_{G1} and V_{G2}, for V_{SD} = 0.5 mV showed a clear honeycomb pattern, which indicates the successful formation of a coupled DQD. In serial DQDs, the current can flow only when the electrochemical potential of each dot is in the bias window. The number of electrons on each dot was fixed inside the hexagonal regions (black regions in Fig. 3.7(a)). At the corners of the hexagons, called triple points, the three charge states degenerate and a current could flow though the DQDs. Ideally, the electrochemical potential of each dot should be independently controllable by each side gate for good performance. However, in the present design of the structure, cross-coupling actually existed and one gate voltage affected both of the dots as shown schematically in Fig. 3.7(b), which displays the equivalent circuit of the present DQD system.

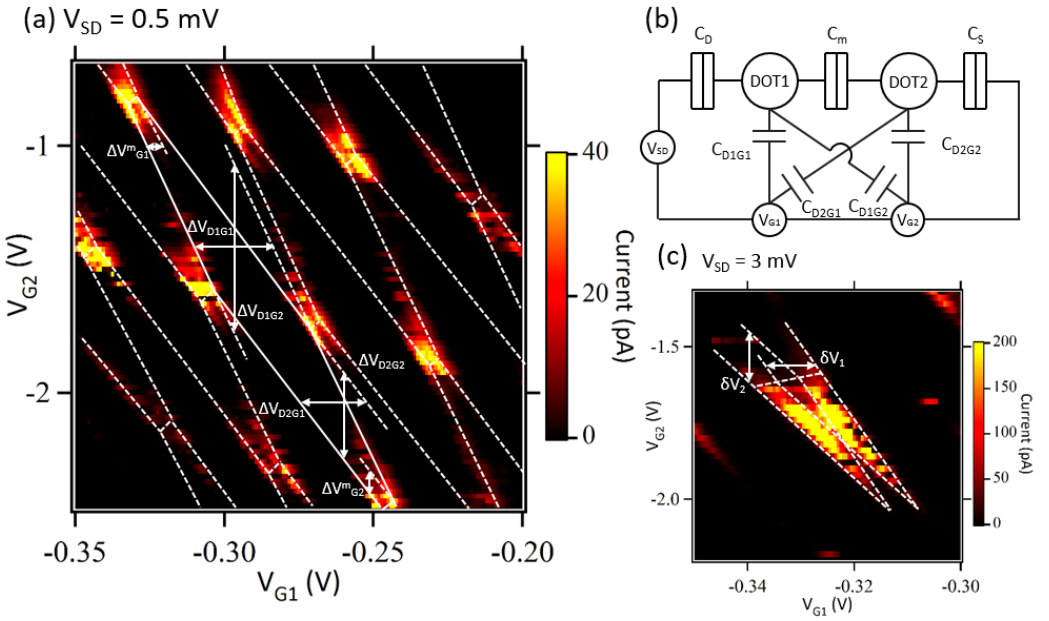

Figure 3.7. Charge stability diagram of a triple barrier sample. The current was measured by sweeping the two side gate voltages at V_{SD} = 0.5 mV. The dotted lines are guides for the eye. The honeycomb pattern indicates the formation of double quantum dots. ΔV_{D1G1}, ΔV_{D1G2}, ΔV_{D2G1}, and ΔV_{D2G2} denote the dimensions of the hexagonal honeycomb cells. ΔV^{m}_{G1} and ΔV^{m}_{G2} are the separations between the adjacent triple points. (b) Equivalent circuit of the double quantum dot system. (c) Bias-triangle at V_{SD} = 3 mV. The dotted lines are guides for the eye. δV_1 and δV_2 indicate the dimensions of the bias triangles used to deduce the conversion factors.

We could calculate the DQD capacitances depicted in Fig. 3.7(b) from experimental parameters (the dimensions of the hexagonal honeycomb cells ΔV_{D1G1}, ΔV_{D1G2}, ΔV_{D2G1}, and ΔV_{D2G2}, the separations of the adjacent triple points ΔV^{m}_{G1} and ΔV^{m}_{G2}) obtained from the honeycomb pattern in Fig. 3.7(a) [1,9-11]. The capacitances ($C_{dot,\ gate}$) between each dot and the side gates were C_{D1G1} ~ 5.5 aF and C_{D2G2} ~ 0.4 aF, and the cross-capacitances were C_{D2G1} ~ 6.7 aF and C_{D1G2} ~ 0.2 aF. The corresponding total capacitances of each dot were C_{1total} ~ 18.4 aF and C_{2total} ~ 23.9 aF, and the interdot capacitance C_m was ~ 5.8 aF. The capacitances between the dots and the MWNT source/drain electrodes, which connected the metal electrodes to the DQD, were C_S ~ 11.0 aF and C_D ~ 6.9 aF, respectively. The corresponding charging energies of each dot derived from C_{1total}, C_{2total}, and C_m were E_{C1} ~ 8.7 meV (101 K) and E_{C2} ~ 6.7 meV (78 K). If we simply assume the resistance value of each barrier to be one third of the total resistance value (161 kΩ / 3 = 54 kΩ), the tunnel barrier height was ~ 3.5 meV, which is roughly estimated from the results in Fig. 3.6. This value is smaller than the obtained charging energies, which is inconsistent; however, we think it is within the variation of the correlation between the barrier height and the room temperature resistance.

When a large bias voltage is applied, the triple point became a finite triangular-shaped region, a so-called bias-triangle. Figure 3.7(c) shows an enlarged bias-triangle of the one in Fig. 3.7(a), measured at V_{SD} = 3 mV. The conversion factors ($\alpha_{dot,\ gate}$) deduced from the dimensions of the bias triangles, δV_1 and δV_2 in Fig. 5.7(c), were α_{D1G1} ~ 8.1 × 10^{-3}, α_{D2G1} ~ 7.4 × 10^{-3}, α_{D2G2} ~ 4.6 × 10^{-4}, and α_{D1G2} ~

3.4×10^{-4} (meV/mV). These conversion factors are much smaller than reported values, for example, for SWNTs [12] and MWNTs [2] with a side gate, and SWNTs [13] and semiconductor nanowires [14,15] with a back gate. The order of magnitude difference between the present conversion factors for the two side gates is thought to have been caused by misalignment of the tunnel barriers and the gate electrodes. Additionally, we know that the gate efficiency can strongly depend on how well the MWNT is stuck to the substrate, which may be another reason.

3.5 Summary

We have evaluated tunnel barriers formed in MWNTs using an Ar atom beam irradiation process. The resistance increase caused by the irradiation varied greatly from sample to sample. We suggest that this is related to the height of the formed tunnel barrier, assuming that the barrier had a simple rectangular shape. Despite the large variations in resistance, some of them were appropriate for tunnel barriers of QDs. A honeycomb-shaped charge stability diagram was observed by measuring the current in triple-barrier samples as a function of different gate voltages. This result indicated the successfully formation of DQDs in the MWNT, demonstrating the potential of our technique towards the at-will fabrication of QD-based functional devices. The technique could be improved to a practically available level by investigating the microscopic nature of the produced damage, and exploring further treatment of the damage.

Reference

[1] W. G. van der Wiel, S. De Franceschi, J. M. Elzerman, T. Fujisawa, S. Tarucha, and L. P. Kouwenhoven, Rev. Mod. Phys. **75**, 1 (2002).

[2] M. Suzuki, K. Ishibashi, T. Toratani, D. Tsuya, and Y. Aoyagi, Appl. Phys. Lett. **81**, 2273 (2002).

[3] R. Martel, V. Derycke, C. Lavoie, J. Appenzeller, K. K. Chan, J. Tersoff, and Ph. Avouris, Phys. Rev. Lett. **87**, 256805 (2001).

[4] R H. Fowler and L. Nordheim Proc. R Soc. A **119,** 173 (1928).

[5] J. M. Beebe, B. Kim, J. W. Gadzuk, C. D. Frisbie, and J. G. Kushmerick, Phys. Rev. Lett. **97**, 026801 (2006).

[6] J. M. Beebe, B. Kim, C. D. Frisbie, and J. G. Kushmerick, ACS Nano **2**, 827 (2008).

[7] H, Song, Y. Kim, Y. H. Jang, H. Jeing, M. A. Reed and T. Lee, Nature **462**, 1039 (2009).

[8] E. H. Huisman, C. M. Guédon, B. J. van Wees, and S. J. van der Molen, Nano Lett. **9**, 3909 (2009).

[9] V. Hung Nguyen, V. Lien Nguyen, and H. Nam Nguyen, J. Appl. Phys. **96**, 3302 (2004).

[10] B.-K. Kim, M. Seo, S. U. Cho, Y. Chung, N. Kim, M.-H. Bae, and J.-J. Kim, Nanotechnology **25**, 295201 (2014).

[11] D. Taubert, D. Schuh, W. Wegscheider, and S. Ludwig, Rev. Sci. Instrum. **82**, 123905 (2011).

[12] C. Meyer, J. M. Elzerman, and L. P. Kouwenhoven, Nano Lett. **7**, 295 (2007).

[13] Y. Kawano, T. Fuse, S. Toyokawa, T. Uchida, and K. Ishibashi, J. Appl. Phys. **103**, 034307 (2008).

[14] S. Huang, N. Fukata, M. Shimizu, T. Yamaguchi, T. Sekiguchi, and K. Ishibashi, Appl. Phys. Lett. **92**, 213110 (2008).

[15] S. Huang, S. K. Shin, N. Fukata, and K. Ishibashi, J. Appl. Phys. **109**, 036101 (2011).

Chapter 4

Tunnel barrier formation by using focused ion beam technique

This chapter will describe tunnel barriers fabricated in individual multi-wall carbon nanotubes (MWNTs) by the Ga focused ion beam irradiation. It is shown that the barrier height has a strong correlation with the barrier resistance that is controlled by the ion dose. Possible origins for the variation in observed barrier characteristics are discussed. Finally, the single electron transistor with two barriers is demonstrated.

4.1 Introduction

Ion or atom irradiation has been employed to fabricate the tunnel barrier in the MWNTs [1,2], and a single QD [1] and coupled QDs (chapter 3) have actually been fabricated with tunnel barriers formed by uniform irradiation through narrow resist

openings. However, the device yield is still low (chapter 3) probably because the width of the barrier is relatively large (~50 nm), limited by a resolution in the e-beam lithography, and microscopic details of the potential profile is not well controlled. In this study, the Ga focused ion beam (FIB) was employed to increase the yield and to control the barrier parameters by forming a narrower barrier. The characteristics of the fabricated barrier were evaluated by measuring temperature and bias-voltage dependence of current through an individual MWNT with a single irradiated region. This technique was applied to fabricate single QDs, and regular Coulomb diamonds that showed a formation of the single QD were obtained with much higher yield than with a resist opening technique.

4.2 Experimental

The MWNT sample was prepared as explained in chapter 2. The MWNT channel was single-scanned perpendicular to the MWNT by the FIB accelerated with 40 kV. The typical irradiation dose used to form the tunnel barriers shown in the later section was 1×10^{16} ions/cm^2 and the number of atoms hit the MWNT was estimated at about 10^4 ions. In addition, a dose of 1.3×10^{13} ions/cm2 was irradiated in this process for taking a scanning ion microscope picture. The inset of figure 4.2 displays a schematic cross-sectional view of the sample structure with a single irradiated region. Two-terminal resistance measurements at room temperature were carried out in a probe station connected to a source-measure unit. The current-voltage (I-V) characteristics at low temperatures were measured in a ^{4}He cryostat.

From the *I-V* curves of non-irradiated samples, we can say that the metal-MWNT junctions were ohmic even at low temperatures down to 1.5 K and the effect of the defects or the impurities in MWNTs on the transport properties was small in the present temperature range.

4.3 Characterization of single barriers

4.3.1 Resistance change

First, we focus on samples with a single irradiated region to characterize the tunnel barrier. The barrier resistance, R_{barrier}, can be defined by the resistance increase after the irradiation. The variation in R_{barrier} after the FIB irradiation is shown in a histogram in Fig. 4.1. It is clear that the resistance variation is much reduced by using the FIB irradiation technique, compared with the barriers fabricated by the resist opening technique presented in chapter 4.

In Fig. 4.2, R_{barrier} is plotted as a function of a Ga-ion dose. There is an obvious tendency that R_{barrier} increases as the ion dose is increased. Although the irradiation was made for different MWNTs which can have a different diameter, the barrier resistance variation in the samples irradiated with a same dose condition can be attributed to fluctuations in the microscopic details of the irradiated region that produce variations in the potential profile of the tunnel barrier.

4.3.2 I-V_{SD} characteristics at various temperatures

Transport measurements were carried out in a liquid He refrigerator to

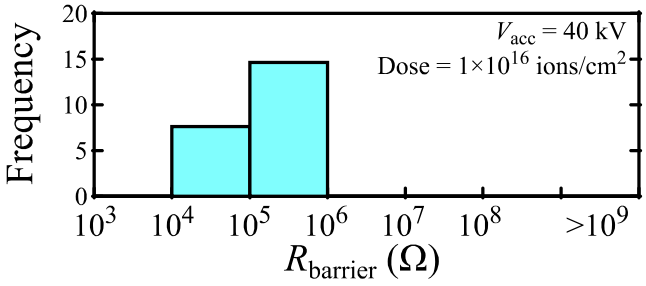

Figure 4.1. Histogram of the variation in the resistance increase ($R_{barrier}$) for 23 samples after the irradiation using the FIB irradiation technique.

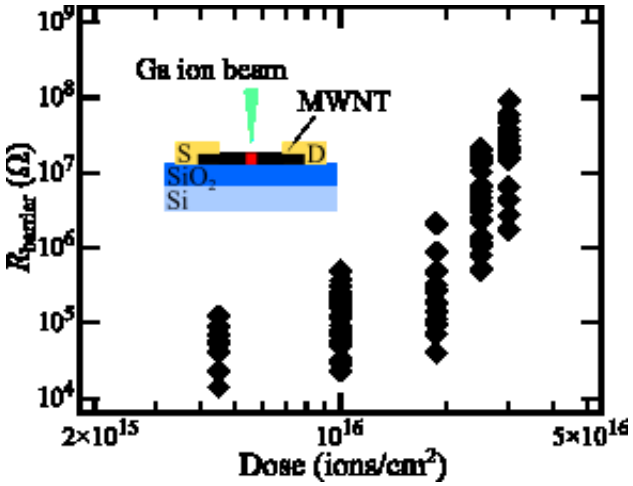

Figure 4.2. $R_{barrier}$ as a function of ion dose. Inset: schematic cross-sectional view of the single-barrier sample.

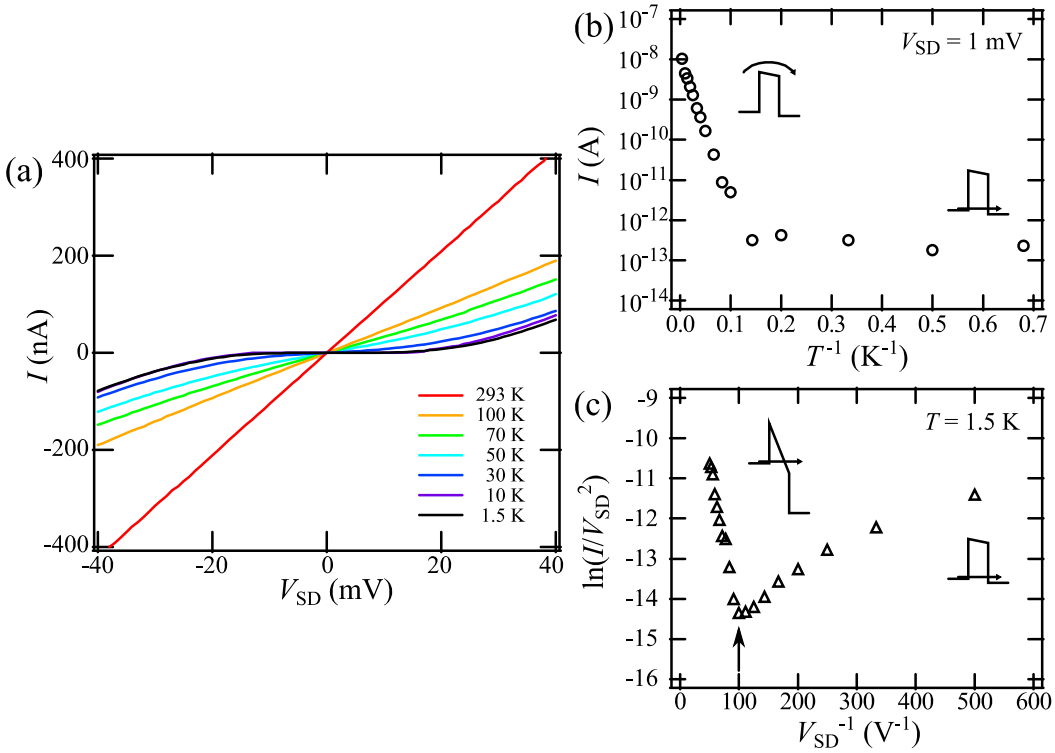

Figure 4.3. (a) I-V_{SD} curves at various temperatures from 1.5 to 293 K. (b) Current in a logarithmic scale as a function of T^{-1} (Arrhenius plot). (c) ln (I / V_{SD}^2) plotted as a function of V_{SD}^{-1} (Fowler-Nordheim plot). The point where the inflection occurs is defined as V_{trans}. These data are taken for a sample with a dose condition of 1.0×10^{16} ions/cm^{-2} and with $R_{barrier} = 89$ kΩ.

characterize the tunnel barriers formed by the FIB irradiation. Figure 4.3 (a) shows I-V_{SD} curves for a typical sample of which $R_{barrier}$ was 89 kΩ measured at various temperatures from 1.5 K to 293 K. The I-V_{SD} curves become non-linear as temperature is decreased. The behaviors have qualitatively been understood by considering the two current components, the direct tunnel current and the thermally activated over-the-barrier current [3,4]. By carefully analyzing temperature and bias voltage (V_{SD}) dependence of these currents, height of the tunnel barrier can be estimated.

4.3.3 Temperature dependence

In Fig. 4.3 (b), a current at a small V_{SD} of 1 mV is plotted in a logarithmic scale as a function of inverse temperature (Arrhenius plot). As seen in the figure, it is almost constant at low temperatures while it increases exponentially above ~10K. At the low temperatures, the temperature-independent direct current is dominant, but the over-the-barrier current becomes more important at higher temperatures. The behaviors at high temperatures can be modeled by the simple thermionic emission. Although the theoretical expression includes a dimension-dependent pre-factor to the exponential term [5,6], we reasonably neglect it because the exponential factor dominates the temperature dependence [3] and assume the simple expression as $I \propto \exp(-\Phi/k_B T)$. From this, we get Φ ~ 11 meV using the data points above 50 K.

4.3.4 Bias voltage dependence

The barrier height can be also estimated by analyzing I-V_{SD} curves at the lowest temperature of 1.5 K where the thermal activation current is neglected. Figure 4.3 (c) displays a so-called Fowler-Nordheim (FN) plot [7]. There are two distinct regions below and above a transition voltage indicated as V_{trans}. At zero bias voltage, the rectangular barrier is assumed. When the bias voltage increases, the barrier forms a trapezoidal shape. In this region, electrons can only flow by a direct tunneling. When the bias voltage becomes larger than the tunnel barrier height, the shape of the barrier becomes triangular and the transport mechanism changes to the FN field emission, as shown in the left inset of Fig. 4.3 (c). In the simplest approximation, V_{trans} could be a reasonable estimate of the barrier height. This analysis is called transition voltage spectroscopy and has been used to investigate the molecular junctions [8-10]. In contrast to the asymmetries in the I-V_{SD} curves observed in the molecular junctions, they are symmetric in the present barriers, as seen in figure 4.3 (a), resulting in the polarity independent V_{trans}. This suggests that the barrier is likely to have a simple rectangular shape.

4.3.5 Barrier height estimation

Figure 4.4 shows the barrier height estimated by the two methods as a function of $R_{barrier}$. The data obtained by the two methods show good agreement for $R_{barrier}$ smaller than ~100kΩ, but appear to show discrepancy for the larger $R_{barrier}$. To consider $eV_{trans} = \Phi$ may be too simplified as further study is necessary to justify

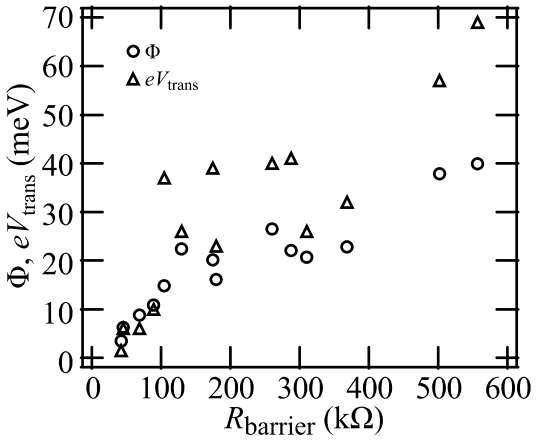

Figure 4.4. Barrier heights estimated by two methods as a function of $R_{barrier}$. In the simple model, eV_{trans} corresponds to the barrier height and shows the larger data scatterings than Φ estimated from the Arrhenius plot.

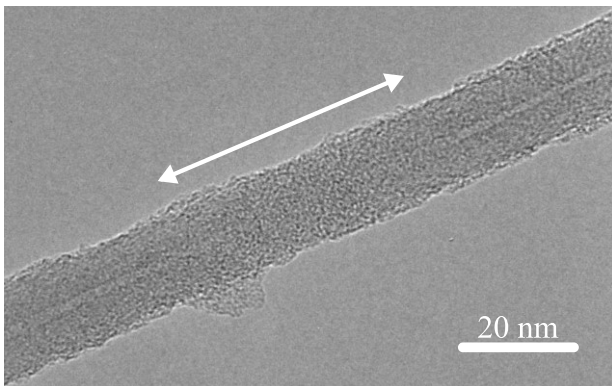

Figure 4.5. Transmission electron microscope image of the irradiated region indicated by the arrow. The FIB irradiation was carried out for the MWNTs dispersed on a TEM grid. A dose condition was 1.5×10^{16} ions/cm^{-2}.

the use of the transition voltage spectroscopy to estimate the barrier height [11]. Apart from further arguments on the true value of the barrier height, there is a clear tendency that the barrier height increases as $R_{barrier}$ is increased. It is important to note that the barrier height can be larger than the room temperature energy (26 meV at 300 K), which indicates usefulness of the present barrier for room temperature applications.

4.4 Characterization of irradiated area by transmission electron microscope

To discuss further about the characteristics of the tunnel barrier, we show in Fig.4.5 a transmission electron microscope (TEM) image of the irradiated region. The MWNT was irradiated with a single-scanned FIB with a typical dose for the barrier formation. It can be seen that the irradiated region indicated by the dotted arrow shows amorphous-like uniform structures. This observation appears to be consistent with a previously reported work [12]. Besides, there is no clear indication of the thinning of the tube by sputtering which was the case for the low-energy Ar ion irradiation [1]. A similar FIB irradiation technique was used to form a tunnel barrier with much larger doses ($>1 \times 10^{17}$ cm^{-2}) than those used in the present experiments [2]. They suggested that a physical trench was formed in the MWNT, which produced the tunnel barrier. However, we do not observe such a trench in Fig. 4.5, and we can assume the irradiated region nearly forms a simple tunnel barrier

with a rectangular shape. It should be noted that the FIB irradiation was carried out for the suspended MWNT on a grid for the TEM observation, which should be compared to the practical case where the irradiation was carried out for the MWNT on a substrate. In this case, some incident ions were reflected back to the MWNT, which might produce a gentler boundary between damaged and undamaged regions. These uncontrolled factors may make the practical barrier more or less deviated from a simple rectangular profile and produce statistical variations in the height and the width of the barrier. Ion trajectories in the MWNT on the substrate also need to be simulated in further study to understand more about the irradiation region.

4.5 Single electron transport through double barrier

Having discussed about the possible variations of the characteristics of the tunnel barriers formed with the present technique, we used it to fabricate single QDs with double barriers. For the Coulomb blockade to be effective, minimum requirements are the barrier resistance enough larger than the quantum resistance (h/e^2 ~ 25.8 kΩ) to suppress quantum fluctuations of charges and the charging energy enough larger than the temperature to suppress the thermal fluctuations [13]. Therefore, the resistance variation may not be a serious problem once the resistance becomes much larger than h/e^2. Individual MWNTs were irradiated at two positions separated by 100 nm and a heavily doped substrate was used as a gate. The regular coulomb diamonds are observed as shown in figure 4.6 (a) and the periodic Coulomb oscillations are observed in figure 4.6 (b), indicating that a single QD is

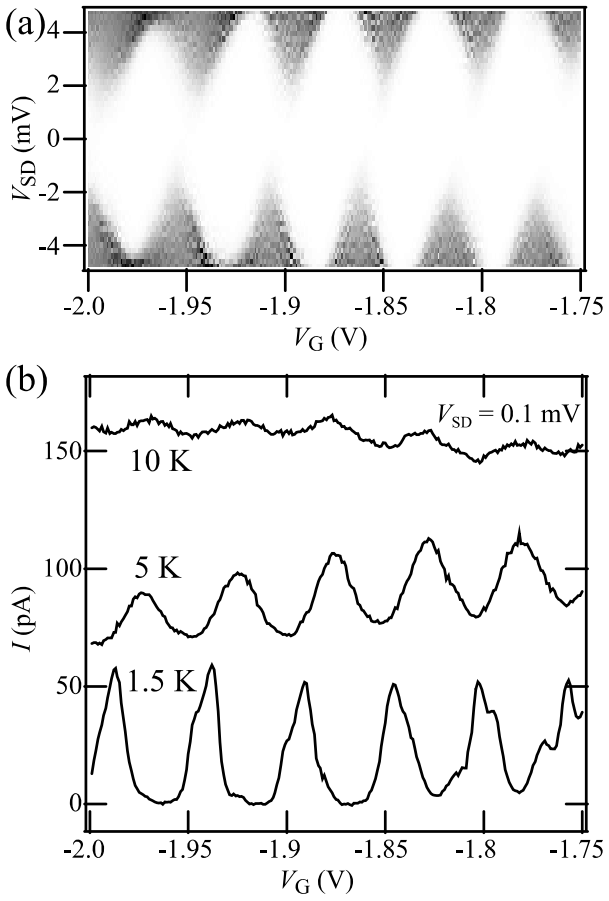

Figure 4.6. (a) Grey scale plot of differential conductance as function of V_{SD} and V_G (Coulomb diamonds) at 1.5 K and (b) Coulomb oscillations of a double-barrier sample. The distance between the two barriers was 100 nm, and the dose condition was 1.2×10^{16} ions cm^{-2} for both barriers. Resistance increase at room temperature, which includes two barriers, was 124 kΩ. The oscillations have shifted during the temperature change between 1.5 and 5 K. This is sometimes observed in the single electron transistor.

really formed. The charging energy is E_c ~ 5 meV, and the gate capacitance is C_g ~ 3.5 aF. A simple cylinder-on-substrate model gives C_g = 5.8 aF for r = 10 nm and L = 100 nm, where r is a radius and L is a length of the cylinder. Considering the fact that the real length for the dot is smaller than the designed length, L, due to the finite width of the barrier, the agreement is good, which indicates that an entire MWNT between the two irradiated regions behaves as a single QD. The Coulomb oscillations are observable up to ~10 K (0.9 meV) which is also consistent with the estimated E_c. The Coulomb peak shift observed in figure 4.6 (b), which is sometimes observed in QDs, is possibly related to the charge fluctuation of traps in the environment which is most likely a substrate. A yield to obtain the single QD behaviors has increased very much compared with previous techniques, however, we have to admit that it is still not high enough up to ~40% in the present fabrication process. Figure 4.7 shows regular Coulomb oscillations of several samples that showed single-dot behaviors. Figure 4.8 shows irregular Coulomb peaks called stochastic Coulomb blockade [14]. The behavior indicates unwanted tunnel barriers were also formed in the channel of the MWNT. The irregular peaks are observed because each of dots has different charging energy and is connected to the same gate voltage through the different capacitances. We could also point out effects of charge traps and impurities that may exist on the substrate and those would work remotely to produce a random potential in the MWNT. This is also a problem for the shift of the Coulomb oscillations, and should be solved by preparing a clean substrate.

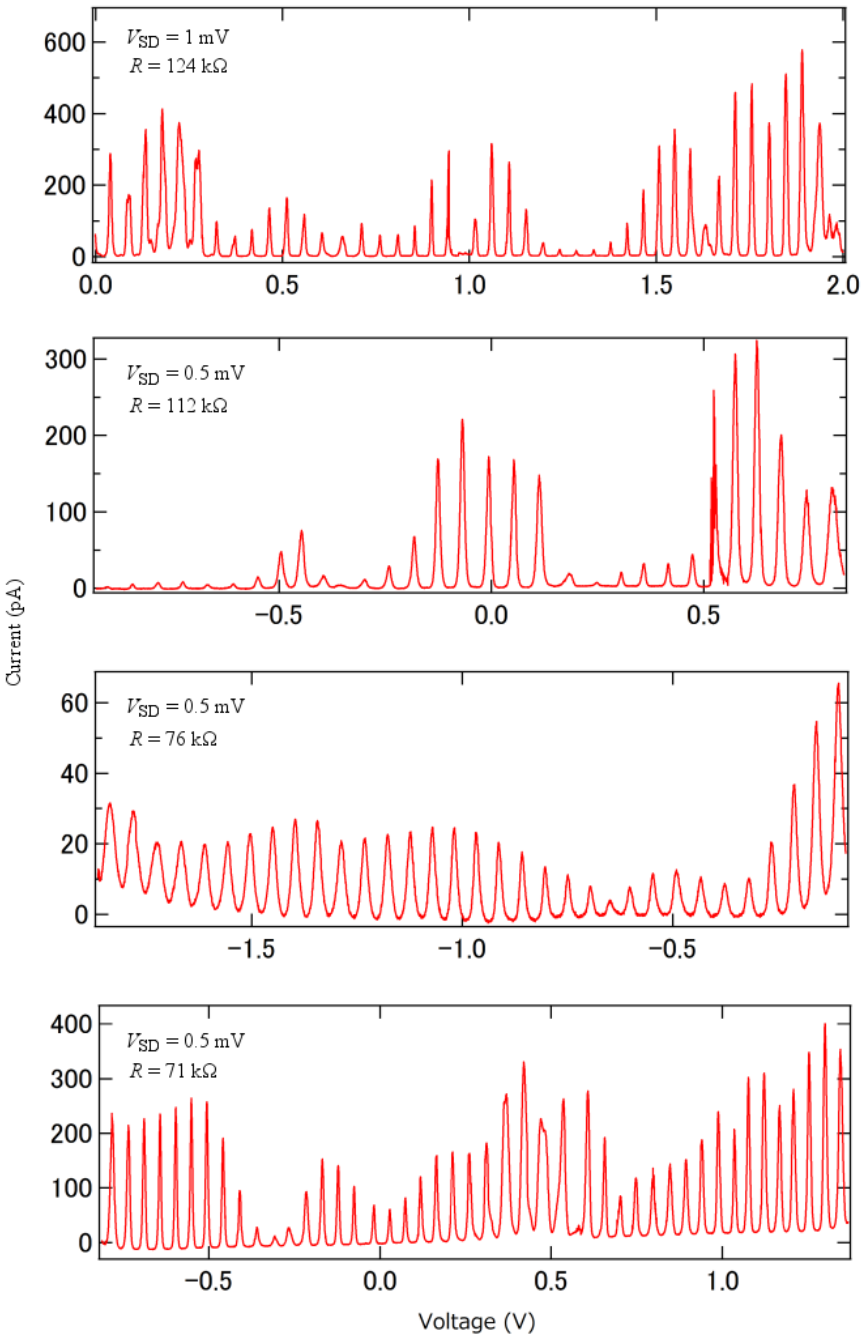

Figure 4.7. Coulomb oscillations of 4 different samples that showed single-dot behaviors.

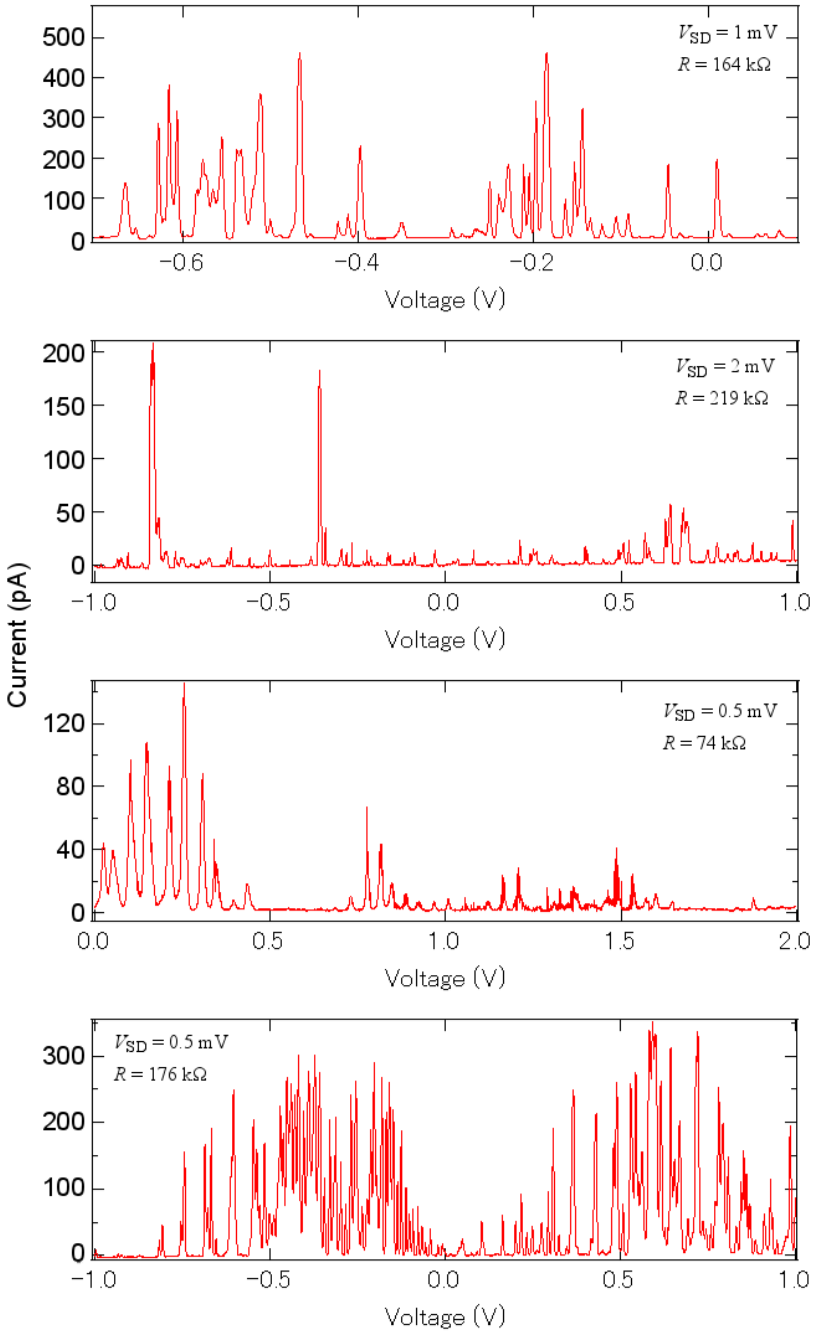

Figure 4.8. Irregular Coulomb peaks that showed multi-dot behaviors

4.6 Summary

We have evaluated tunnel barriers in a MWNT channel formed by the FIB irradiation technique. The variation of the barrier resistance after the irradiation was reduced very much compared with that in the resist opening technique in chapter 3. It was shown that the barrier resistance was controlled with some variations by the dose condition, and the estimated barrier height had a strong correlation with the barrier resistance. We could fabricate single electron transistors with a yield up to ~40 %, and would suggest that further improvements are possible by carefully preparing a clean substrate and the present technique is useful to fabricate integrated nanodevices and circuits with multiple QDs.

Reference

[1] M. Suzuki, K. Ishibashi, T. Toratani, D. Tsuya, and Y. Aoyagi, Appl. Phys. Lett. **81**, 2273 (2002).

[2] Y. Kurokawa, Y. Ohno, S. Kishimoto, T. Okazaki, H. Shinohara and T. Mizutani, Jpn. J. Appl. Phys. **43**, 5669 (2004).

[3] R. Martel, V. Derycke, C. Lavoie, J. Appenzeller, K. K. Chan, J. Tersoff, and Ph. Avouris, Phys. Rev. Lett. **87**, 256805 (2001).

[4] M. Poot, E. Osorio, K. O'Neil, J. M. Thijssen, D. Vanmaekelbergh, C. A. van Walree, L. W. Jenneskens, and H. S. J. van der Zant, Nano Lett. **6**, 1031 (2006).

[5] A. Anwar, B. Nabet, J. Culp, and F. Castro, J. Appl. Phys. **85**, 2663 (1999).

[6] J. Appenzeller, M. Radosavljević, J. Knoch, and Ph. Avouris, Phys. Rev. Lett. **92**, 048301 (2004).

[7] R. H. Fowler and L. Nordheim, Proc. Royal Soc. London, Series A **119**, 173 (1928).

[8] J. M. Beebe, B. Kim, J. W. Gadzuk, C. D. Frisbie, and J. G. Kushmerick, Phys. Rev. Lett. **97**, 026801 (2006).

[9] J. M. Beebe, B. Kim, C. D. Frisbie, and J. G. Kushmerick, ACS Nano, **2**, 827 (2008).

[10] H. Song, Y. Kim, Y. H. Jang, H. Jeing, M. A. Reed, and T. Lee, Nature, **462** 1039 (2009).

[11] E. H. Huisman, C. M. Guédon, B. J. van Wees, and S. J. van der Molen, Nano Lett. **9**, 3909 (2009).

[12] B. Q. Wei, J. D'Arcy-Gall, P. M. Ajayan, and G. Ramanath, Appl. Phys. Lett. **83**, 3581 (2003).

[13] D. V. Averin and K. K. Likharev: Mesoscopic Phenomena in Solids, eds. B. Altshuler, P. A.Lee and R. A. Webb (Elsevier Science Publishers, 1991) Chap.6.

[14] I. M. Ruzin, V. Chandrasekhar, E. I. Levin and L. I. Glazman: Phys. Rev. B **45** 13469 (1992).

Chapter 5

Conclusion

5.1 Comparison of the resistance after irradiation

Figure 5.1 shows the histogram of the resistance after irradiation by using the resist opening technique (a) and the FIB technique (b) shows in chapter 3 and 4, respectively.

In the resist opening technique, one-third samples were broken while the resistance of a few samples did not change at all. We consider the cause of the wide variation is that the width of the barrier is relatively wider of 50 nm, limited by a resolution in the e-beam lithography, and microscopic details of the potential profile is not well controlled. To make narrower barrier in the nanotube, narrower opening in the resist layer is required. However, the yield of the opening itself decrease to make narrower pattern, especially making multiple barrier. Thinner resist layer is

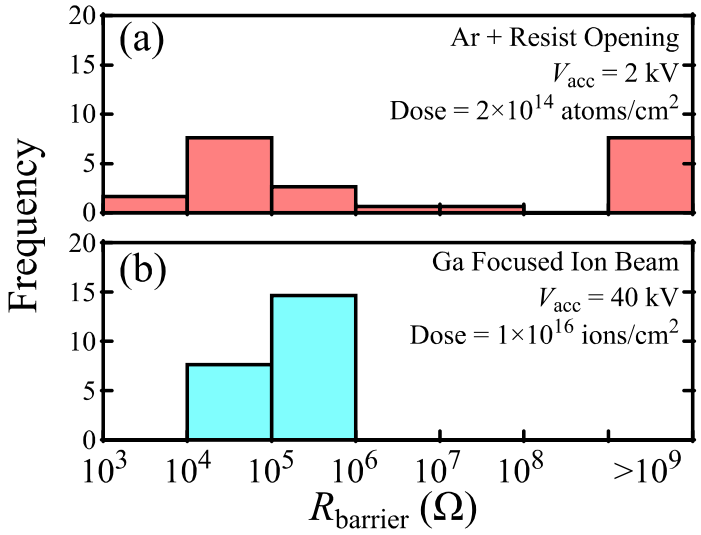

Fig. 5.1. Comparison of the two histograms

also required to make fine patterns but the thin layer cannot give sufficient protection against the beam irradiation and damaged layer become difficult to remove after the process. A beam with higher acceleration voltage may cause also serious damage on the resist layer. However, the resist opening technique is the same process as photolithography and has a potential for the mass production adaptable process in the future.

In the FIB technique, on the other hand, the resistance had small variation. The reproducibility and controllability was much improved from the resist opening technique. We consider that one of the possible factor of the improvement is the narrower width of the damaged region. Due to the development of the technique, we can make quantum dots with relatively high reproducibility. However, the FIB technique is the same process as electron beam lithography and is not suitable for

mass production.

5.2 Conclusion

In this thesis, we have developed tunnel barrier formation technique in MWNTs. Two irradiation methods, resist opening technique and FIB technique, were examined and demonstrated that the tunnel barriers were successfully formed in MWNTs. In resist opening technique, the barrier resistance after the irradiation was uncontrollable. In FIB technique, on the other hand, the resistance changes were reasonably reproducible and showed ion dose dependence with some variation. The height of the formed tunnel barriers was estimated from Arrhenius plot and the Fowler-Nordheim plot. For both estimation methods, the barrier height had a strong correlation with the barrier resistance. In the FIB technique, in particular, the controllability of the barrier height by the ion dose through the barrier resistance was presented. As the first step application of these techniques, the single quantum dots by the FIB technique and the coupled quantum dots by the resist opening technique were successfully demonstrated. In particular, single-dot behaviors were observed with high enough reproducibility for device fabrication of four tenths by FIB technique. These results suggest that the present techniques for tunnel barrier formation in the MWNTs are the potential candidate towards the at-will fabrication of integrated single electron transistor circuits.

5.3 Future work

At the present stage, we have not observed discrete quantum levels even at 1.5 K with the dot length of 100 nm. One of the requirements to observe discrete levels is that the energy separation becomes larger than the temperature energy. In previous study [1], discrete quantum levels in MWNT quantum dots by resist opening technique have been reported with the dot length of less than 100 nm. We have tried to make dots with the length of less than 100 nm. However, we could not succeed to make dots with the condition. One of the probable reason is the broad FIB damages the region between tunnel barriers resulting fluctuated potential in the dot. Further development of the technique using narrower ion beam, He ion beam for example, is required.

One of the advantages of FIB technique is that the resist process is not required. Therefore, the technique can form tunnel barriers in suspended MWNTs. Especially, coupled dots can be form in MWNTs. Electromechanical resonators are attractive for high frequency mechanical resonator owing to their mechanical strength and their light mass. The device can be used for high sensitive mass sensor or hybrid system with single electron transport coupled to quantized mechanical vibration.

MWNTs are fascinating material for nanoelectronics and quantum devices. We believe our research will contribute to the future development and investigation.

Reference

[1] D. Tsuya, M. Suzuki, S. Moriyama, Y. Aoyagi, and K. Ishibashi, Physica E, **24**, 50 (2004).